REPORT 1176

DETERMINATION OF MEAN CAMBER SURFACES FOR WINGS HAVING UNIFORM CHORDWISE LOADING AND ARBITRARY SPANWISE LOADING IN SUBSONIC FLOW [1]

By S. Katzoff, M. Frances Faison, and Hugh C. DuBose

SUMMARY

The field of a uniformly loaded wing in subsonic flow is discussed in terms of the acceleration potential. It is shown that, for the design of such wings, the slope of the mean camber surface at any point can be determined by a line integration around the wing boundary. By an additional line integration around the wing boundary, this method is extended to include the case where the local section lift coefficient varies with spanwise location (the chordwise loading at every section still remaining uniform).

For the uniformly loaded wing of polygonal plan form, the integrations necessary to determine the local slope of the surface and the further integration of the slopes to determine the ordinate can be done analytically. An outline of these integrations and the resulting formulas are included.

Calculated results are given for a sweptback wing with uniform chordwise loading and a highly tapered spanwise loading, a uniformly loaded delta wing, a uniformly loaded sweptback wing, and the same sweptback wing with uniform chordwise loading but elliptical span load distribution.

INTRODUCTION

The design of mean camber surfaces to sustain a specified area distribution of lift at subsonic speeds involves basically a relatively straightforward process: a system of bound and trailing vortices is set up in the plane of the wing according to the specified distribution of lift, and the corresponding vertical velocity is calculated, by the Biot-Savart law, at points on the surface where the local slopes are desired. Reasonably practical numerical and graphical procedures have been developed for performing this integration of the velocity due to this distribution of vortices (see, for example, ref. 1). If the chordwise loading is specified to be uniform, as in a number of recent wing-design studies, the problem is basically simplified; as will be shown, the solution can then be reduced from a double integral over the wing area (or over the wing area plus wake area) to a line integral around the boundary of the wing and, in the simplest cases, it can even be reduced to a purely analytical procedure.

The purposes of the present report are to outline the basic theory behind the solution of these problems involving uniform chordwise loading, to summarize the mathematical application of the theory and the development of the required formulas, and to describe the actual use of these derived results in the design of mean camber surfaces for this type of loading.

The basic theory of the uniformly loaded lifting surface is reviewed first. The particular case of the infinitesimally wide, uniformly loaded longitudinal strip is next discussed, together with the integration of such strips to form the wing of arbitrary contour and arbitrary spanwise loading. For the uniformly loaded polygonal wing, closed expressions are derived for both the local slope of the mean camber surface and the local height of the surface (relative to the leading edge). Sections of the mean camber surfaces of four wings calculated by these methods are also presented.

SYMBOLS

x, y, z	streamwise, lateral, and vertical coordinates, respectively (see fig. 1)
x', y'	coordinates of vortex element on wing boundary
U	stream velocity
w	vertical velocity induced by unit vortex (positive upward)
p	pressure
ρ	density
C_L	wing lift coefficient
c_l	wing section lift coefficient
c	chord
$\bar{c}$	average chord
$d\mathbf{s}$	vortex element (vector)
$\mathbf{q}$	vector from vortex element to point
M	Mach number
A	aspect ratio
Λ	sweep angle

Vortex-segment symbols:

(x_1, y_1), (x_2, y_2) end points of vortex segment; $(y_1 > y_2)$

$\alpha = \tan^{-1}\left(\frac{y_1 - y_2}{x_1 - x_2}\right)$

$L = y_1 \csc \alpha$

$M = -y_2 \csc \alpha$

$l = \sqrt{x^2 - 2xL \cos \alpha + L^2}$

$m = \sqrt{x^2 + 2xM \cos \alpha + M^2}$

$s = \sqrt{(x_1 - x)^2 + y_1^2}$

$t = \sqrt{x^2 + y_1^2}$

Subscripts:

LE	leading edge
TE	trailing edge
I, II, III	cases I, II, and III of appendix

[1] Supersedes NACA TN 2903, "Determination of Mean Camber Surfaces For Wings Having Uniform Chordwise Loading and Arbitrary Spanwise Loading in Subsonic Flow" by S. Katzoff, M. Frances Faison, and Hugh C. DuBose, 1953.

368555—56——31

BASIC THEORY FOR UNIFORMLY LOADED WINGS

Application of acceleration potential.—In flow fields consisting of a small perturbation flow superimposed on a uniform flow, the pressure is a potential (multiplied by $-1/\rho$, it is frequently termed acceleration potential) that satisfies Laplace's equation (see, for example, ref. 2, pp. 225–227). In the field of a uniformly loaded lifting surface, then, the pressure (relative to free-stream pressure) is a harmonic potential that must satisfy the following boundary conditions:

(a) It has a uniform negative value over the upper face of the lifting surface.

(b) It has a numerically equal, uniform positive value over the lower face of the lifting surface. (That the upper- and lower-surface pressures are equal and opposite is not, perhaps, obvious merely from the fact that a pressure difference exists across the surface. If, however, the lifting surface is represented by a distribution of bound and trailing vortices, as in ref. 1, this fact is immediately apparent.)

(c) It vanishes at infinity.

These boundary conditions, which uniquely define the pressure throughout the field, are recognized as identical with the conditions on the velocity potential in the field of a closed vortex that coincides with the edge, or boundary, of the lifting surface. Accordingly, the pressure at any point in the field of a uniformly loaded lifting surface is equal in value to the velocity potential of such a vortex, the strength of which is the pressure difference between the upper and the lower faces, or the lift per unit area. Correspondingly, the pressure gradient at any point in the field is equal in both magnitude and direction to the potential gradient (that is, the velocity) associated with this vortex at that point; and it can accordingly be determined by the Biot-Savart law. For present purposes, only the vertical component of this gradient is of interest. The vortex should not, of course, be confused with the lifting vortices of the usual airfoil theory; the latter vortices are not used in the present report.

The vertical acceleration of a fluid particle is $-\frac{1}{\rho}\frac{\partial p}{\partial z}$ (see fig. 1 for coordinate system), so that the vertical velocity acquired by a particle which has come into the neighborhood of the wing from a large distance upstream is the integral of this expression with respect to time, or $\int_{-\infty}^{x} -\frac{1}{\rho}\frac{\partial p}{\partial z}\frac{dx}{U}$, where the factor dx/U is the element of time. (In order to simplify the notation, the same symbol x is used for both the running variable and the upper limit.) All perturbation velocities are assumed to be small so that the path of integration, or the path of the fluid particle, is the line $y=$Constant, $z=$Constant.

Dividing this vertical velocity by U gives the vertical slope dz/dx of the streamline. In particular, if the integral is evaluated for a point on the lifting surface itself, the local slope of the surface is given by $-\frac{1}{\rho U^2}\int_{-\infty}^{x}\frac{\partial p}{\partial z}dx$, where the integration is along the line $y=$Constant, $z=0$. Here again the small-perturbation theory assumes that all displacements from the straight undisturbed streamlines are so small that the path of integration may, with sufficient accuracy, be taken in the plane $z=0$, and, in particular, it assumes that the vertical displacement of the trailing edge relative to the leading edge is so small that the boundary vortex may also be taken in the plane $z=0$. The local height of the surface z, relative to the leading edge, is the integral of this slope, or

$$-\frac{1}{\rho U^2}\int_{x_{LE}}^{x} dx\int_{-\infty}^{x}\frac{\partial p}{\partial z}dx$$

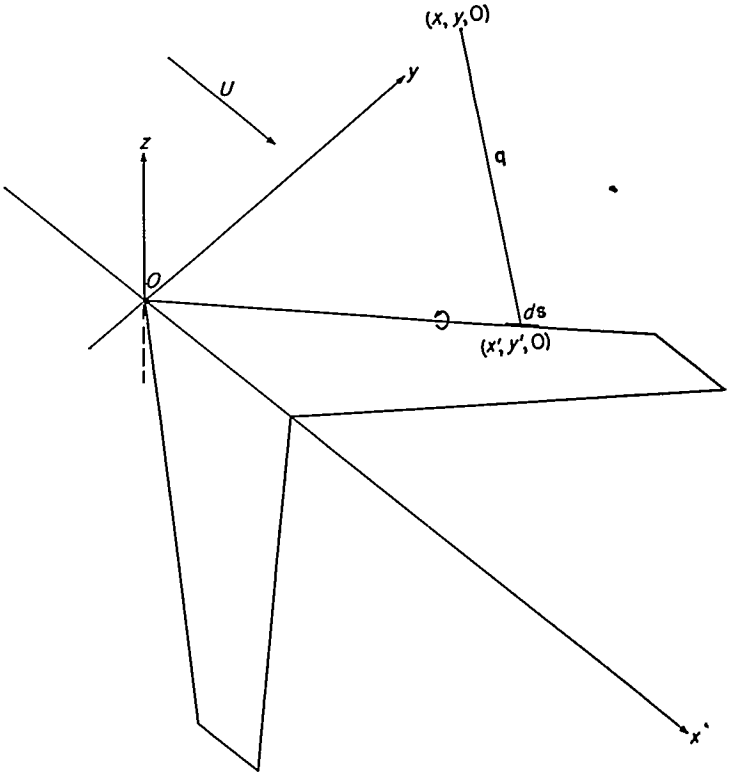

FIGURE 1.—Element of vortex on wing boundary showing coordinate and vector systems used in the application of the Biot-Savart law.

For any lift coefficient C_L the pressure difference across the lifting surface is $\frac{C_L}{2}\rho U^2$, which, as previously noted, is numerically equal to the strength of the vortex that is assumed around the edge of the projected plan form of the lifting surface. Thus, finally, the local slope of the surface is

$$\frac{dz}{dx}=-\frac{1}{2}C_L\int_{-\infty}^{x} w\,dx \qquad (1)$$

where w is the vertical velocity (positive upward) in the plane of the lifting surface induced by a unit vortex along the edge of the surface. The local height of the surface, relative to the leading edge, is then

$$z=-\frac{1}{2}C_L\int_{x_{LE}}^{x} dx\int_{-\infty}^{x} w\,dx \qquad (2)$$

The direction of rotation of the unit vortex is such that its flow is upward through the surface of the wing; that is, the potential increases by unity along a path from the upper to the lower wing surface around the edge of the wing.

Line integral for local slopes of uniformly loaded wing with arbitrary plan form.—By equation (1), the local slope dz/dx may be determined by evaluating the vertical velocity w induced by the entire boundary vortex and then integrating w from $-\infty$ to x. A more convenient method, however,

is to evaluate the contribution to w induced by an infinitesimal element of the bounding vortex, to integrate this contribution from $-\infty$ to x (which is readily done analytically), and then to integrate this result over all the elements of the bounding vortex.

The differential form of the Biot-Savart equation (see ref. 2, p. 167) for the induced velocity $d\mathbf{w}$ due to an element $d\mathbf{s}$ of a unit vortex is

$$d\mathbf{w}=\frac{1}{4\pi}\frac{d\mathbf{s}\times\mathbf{q}}{|\mathbf{q}|^3}$$

where $\mathbf{q}$ is the vector from the vortex element to the point in question, and the direction of $d\mathbf{s}$ is taken as the direction of advance of a right-hand screw rotating in the direction of the circulation about $d\mathbf{s}$ (see fig. 1). For the present problem, where the point lies in the plane of the wing, this induced velocity is in the z-direction and is given by

$$dw=\frac{1}{4\pi}\frac{(y-y')dx'-(x-x')dy'}{[(x-x')^2+(y-y')^2]^{3/2}}$$

where (x, y) is the point at which the induced velocity is desired, and (x', y') is the location of the vortex element (dx', dy') on the wing boundary.

Accordingly, by equation (1), the contribution of a boundary element (dx', dy') of a uniformly loaded wing to the slope of the wing surface at point (x, y) is

$$d\,(\text{Slope})_{(dx',dy')}=-\frac{1}{2}\frac{C_L}{4\pi}\int_{-\infty}^{x}\frac{(y-y')dx'-(x-x')dy'}{[(x-x')^2+(y-y')^2]^{3/2}}\,dx$$

$$=-\frac{C_L}{8\pi}\left[\frac{(x-x')dx'}{(y-y')\sqrt{(x-x')^2+(y-y')^2}}+\frac{dx'}{y-y'}+\frac{dy'}{\sqrt{(x-x')^2+(y-y')^2}}\right]$$

The signs of dx' and dy' are determined from the previously mentioned convention for the direction of the vector $d\mathbf{s}$ (or (dx', dy')); for example, both dx' and dy' are negative for the leading-edge element shown in figure 1.

The net slope of the mean camber surface at the point (x, y) is the integral of the preceding expression around the wing boundary, or

$$\frac{dz}{dx}=-\frac{C_L}{8\pi}\oint\left[\frac{(x-x')dx'}{(y-y')\sqrt{(x-x')^2+(y-y')^2}}+\frac{dx'}{y-y'}+\frac{dy'}{\sqrt{(x-x')^2+(y-y')^2}}\right] \tag{3}$$

where the counterclockwise direction of the integration automatically takes care of the signs. The problem of determining the local slope of the mean camber surface at the point (x, y) is thus reduced to the evaluation of this line integral.

WINGS WITH ARBITRARY PLAN FORM AND ARBITRARY SPANWISE LOADING

Wing considered as sum of uniformly loaded chordwise strips.—For the wing having uniform chordwise loading and arbitrary spanwise loading, it is convenient to consider the wing to be made of a series of uniformly loaded chordwise strips of infinitesimal span. For each such strip (span dy', see fig. 2), the pressure field can be represented by the

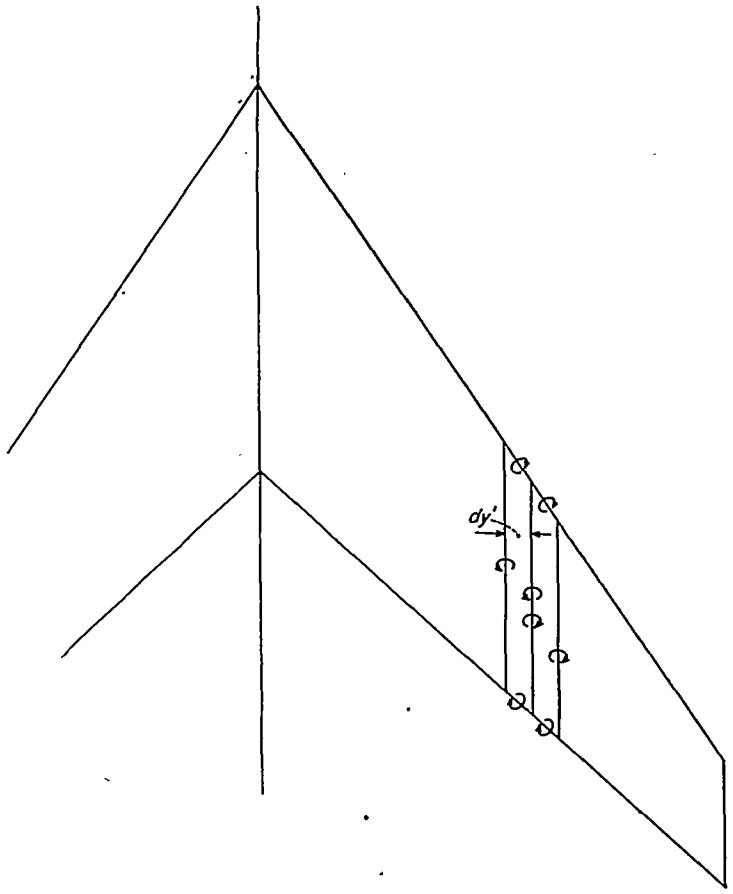

FIGURE 2.—Wing composed of uniformly loaded chordwise strips of span dy' with a closed vortex superimposed on the boundary of each strip.

velocity potential of a closed vortex superimposed on the boundary of the strip. Each of these bounding vortices has strength equal to the local pressure difference Δp between the upper and lower surfaces of the strip.

If, as in the preceding analysis, the spanwise loading is uniform, all these closed vortices will be of the same strength, so that the chordwise segments common to any two adjacent strips cancel and only those vortex elements lying on the boundary of the wing remain. The result is thus the same as that previously discussed for the uniformly loaded wing (eq. (3)).

If, however, the spanwise loading is not uniform, the closed vortices surrounding adjacent strips will be of unequal strength; vortex segments common to adjacent strips will no longer cancel, and vortex elements lying on the wing boundary will vary in strength along the boundary. The contribution of these boundary vortex elements to the induced velocity w can still be summed by a line integration around the wing boundary of the expression given in equation (3), except that C_L must be replaced by the local section lift coefficient $c_l(y')$ and placed under the integral sign. The contribution of the chordwise segments is derived in the following paragraph.

Streamwise vortex segments.—The Biot-Savart formula for the induced velocity due to the straight-line chordwise vortex segment of unit strength is

$$w=\frac{1}{4\pi r}(\cos\theta_2+\cos\theta_1) \tag{4}$$

where r, θ_1, and θ_2 are defined in figure 3. With r and the cosines expressed in Cartesian coordinates, this expression becomes

$$w=\frac{1}{4\pi(y-y')}\left\{\frac{x-(x'+c)}{\sqrt{[x-(x'+c)]^2+(y-y')^2}}-\frac{x-x'}{\sqrt{(x-x')^2+(y-y')^2}}\right\}$$

where c is the local chord. The integral of this expression from $-\infty$ to x, multiplied by $-dc_l/2$ or $-\frac{1}{2}\frac{dc_l}{dy'}dy'$ (see eq. (1)), gives the contribution to the slope from the streamwise vortex segment of strength corresponding to dc_l and length equal to the local chord:

$$d(\text{Slope})=-\frac{1}{8\pi(y-y')}\frac{dc_l}{dy'}dy'\left([\sqrt{(x-x')^2+(y-y')^2}+(x-x')]-\right.$$
$$\left.[\sqrt{\{x-(x'+c)\}^2+(y-y')^2}+x-(x'+c)]\right)$$

Finally, integrating this last equation with respect to y' across the span of the wing (from left to right) gives the contribution of all these chordwise segments to the slope at the point (x,y). It will be observed, however, that the term within the second bracket in this equation is the same as that within the first bracket except that x' is replaced by $x'+c$, the corresponding trailing-edge coordinate. Accordingly, the integral of this expression across the span can, for convenience, be considered as the line integral

$$\frac{1}{8\pi}\oint\frac{dc_l}{dy'}dy'\frac{1}{y-y'}[\sqrt{(x-x')^2+(y-y')^2}+(x-x')] \qquad (5a)$$

or

$$\frac{1}{8\pi}\oint dc_l\frac{1}{y-y'}[\sqrt{(x-x')^2+(y-y')^2}+(x-x')] \qquad (5b)$$

around the boundary of the wing.

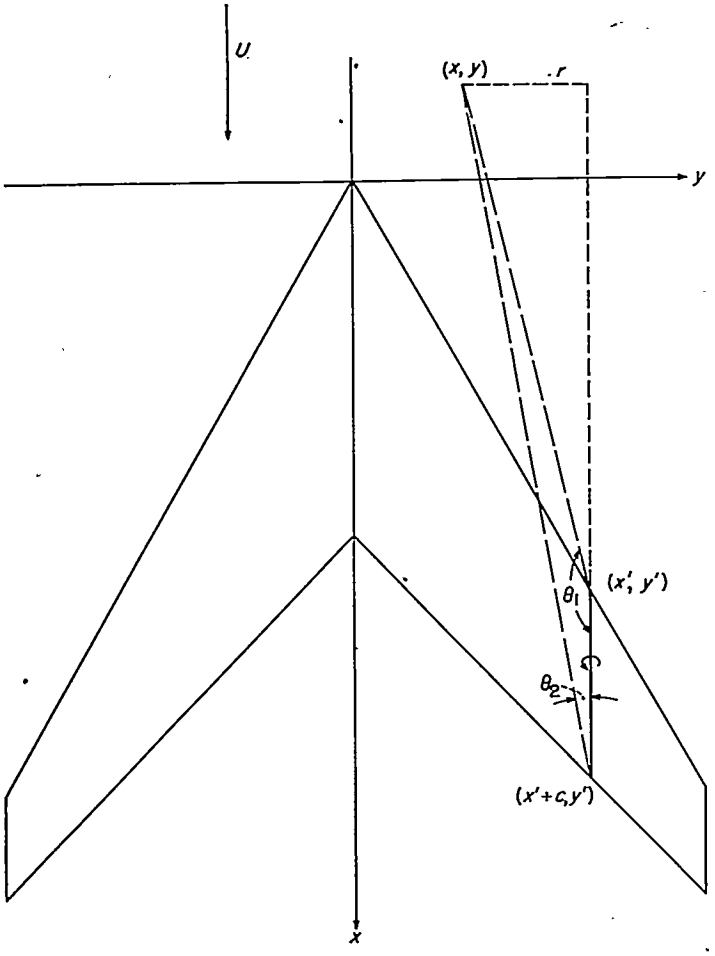

FIGURE 3.—Geometrical relationships for straight-line chordwise vortex segments that occur with spanwise-varying area loading.

The problem of determining the local slope of the mean camber surface at point (x,y) is thus reduced to the evaluation of the line integrals (3) and (5), where the integral (5) is omitted if there is no spanwise variation in the area loading (or in the local lift coefficient c_l) and where the local lift coefficient c_l replaces C_L in equation (3) and must be brought under the integral sign if there is a spanwise variation of c_l.

COMPUTATION

Although computing the integrands of expressions (3) and (5) and then performing the integrations should be a fairly straightforward process, a short outline of suggested procedures may be helpful. It may be noted at the beginning that, since the slopes (and the integrals for the slopes) are nondimensional, the results will be independent of the dimensional scale chosen for the work; taking the root chord or the semispan as unity will probably be most convenient. It may also be remarked that a carefully drawn plan form of the wing will be helpful in setting up the computations.

Résumé of procedure for computing slopes of uniformly loaded mean camber surface.—Given the plan form of a wing that is to have uniform area loading and a specified lift coefficient, a possible procedure is as follows:

(1) Select points (x,y) on the surface where the slopes are to be obtained. In general, these points should lie along several selected chord lines, with perhaps four along each line.

(2) Select points (x',y') along the leading and trailing edges where the integrands of equation (3) are to be determined. In general, trailing-edge points should be at the same spanwise positions as the leading-edge points.

(3) Consider the integral in equation (3) to be broken up into two parts—one with respect to x' and one with respect to y':

$$\oint\frac{1}{y-y'}\left[\frac{x-x'}{\sqrt{(x-x')^2+(y-y')^2}}+1\right]dx' \qquad (6a)$$

and

$$\oint\frac{dy'}{\sqrt{(x-x')^2+(y-y')^2}} \qquad (6b)$$

For each point (x,y), compute the values of the integrands in expressions (6a) and (6b) for all the (x',y') points.

(4) For each point (x,y), plot the integrands of (6a) against x', plot the integrands of (6b) against y', and determine the

area of each (for example, by running the planimeter around the curve in the direction corresponding to a counterclockwise movement of the variable point (x',y') around the wing boundary).

(5) For each point (x,y), sum these two areas and multiply by $-C_L/8\pi$ in order to determine the local slope dz/dx.

(6) The actual heights of the mean camber surface along the chosen chords are now determined by integrating the slopes found in the preceding steps. The integration cannot extend quite to the leading and trailing edges, however, because the slopes cannot be readily determined very close to the ends of the chord lines, where the slopes become infinite. Near the ends, however, the mean camber lines of the sections may be considered as NACA $a=1.0$ mean lines (ref. 3), and they may accordingly be filled in, with generally adequate accuracy, by fitting NACA $a=1.0$ mean lines between the front and rear limits of the calculated segments of the mean camber lines and the leading and trailing edges.

The integral (6a) is actually improper, since the integrand becomes infinite where $y'=y$. The Cauchy principal value exists, however, and is evaluated by first adding the integrands at equal distances but on opposite sides from the singular point and then integrating the sum. This method will be further described in a subsequent section.

Résumé of procedure for computing slopes of a mean camber surface with uniform chordwise loading and arbitrary spanwise loading.—For an arbitrary spanwise loading, an additional integration is required, together with a modification of the preceding integrations.

(1) Determine the integrals

$$\oint \frac{c_l}{y-y'}\left[\frac{x-x'}{\sqrt{(x-x')^2+(y-y')^2}}+1\right]dx' \tag{7a}$$

and

$$\oint \frac{c_l dy'}{\sqrt{(x-x')^2+(y-y')^2}} \tag{7b}$$

by the same process as was used for (6a) and (6b), except that c_l, being now a variable, must be brought inside the integral.

(2) Determine the spanwise rate of change of local lift coefficient dc_l/dy' at points y'. Compute values of the integrand in

$$\oint \frac{dc_l}{dy'}\frac{1}{y-y'}\left[\sqrt{(x-x')^2+(y-y')^2}+(x-x')\right]dy' \tag{8}$$

Plot against y' and integrate. This integral is also improper and is treated as previously mentioned.

(3) For each point (x,y), the local slope dz/dx is

$$\frac{1}{8\pi}\left[\text{Integral (8)}-\text{Integral (7a)}-\text{Integral (7b)}\right]$$

Example.—In figure 4 is shown the plan form of a swept wing and the desired spanwise lift distribution. As an example of the computation, integrals (7a), (7b), and (8) will be obtained for the point designated P in the figure. Points designated a . . . z and a′ . . . z′ are the points on the boundary where the integrands were evaluated; the primed symbols are used merely because more than 26 symbols were needed. The origin was taken at the wing apex and the wing semispan was assumed equal to unity.

The computation of the integrands at the points around the boundary is given in table I. Most of the points were evenly spaced, but near the singularity $(y'=y)$, the intervals were reduced to one-tenth as much as most of the other intervals.

Figure 5 shows the plots of the integrands (multiplied by $1/8\pi$ or $-1/8\pi$) against x' or y' and also shows the method of determining the Cauchy principal value at the singularity. For example, in figure 5(c) it will be seen that the integrand goes to ∞ at the right of the singularity and to $-\infty$ at the left of the singularity. Algebraically adding the integrands at equal distances from the singularity (for example, the value at point b plus the value at point v, the value at point c plus the value at point u, and so on) and plotting the sum results in the section Bl of the curve, where the portion nearest the singularity is obtained by extrapolation from point k. The desired integral (8) is finally determined by running the planimeter along the path abBlLVva′b′j′r′s′a.

As a further example of the intermediate steps in the calculation of a mean camber surface, figure 6(a) is shown, which is a plot of the slope dz/dx along the streamwise chord through point P. The example calculation described in the preceding paragraphs, it will be noted, gives the three integrals the sum of which provides one point on this dz/dx curve of figure 6(a). In figure 6(b) is shown the corresponding curve for the NACA $a=1.0$ mean line, for $c_l=1.0$, from reference 3. The curve may be found useful in extrapolating to the leading and trailing edges, as previously mentioned.

As may be inferred from the preceding résumé of the computations for one point P, the total effort required to compute accurately a mean camber surface by the method described is very large, although, according to the authors' experience, it is not at all prohibitive. Nevertheless, the work is ideally suited to modern high-speed computing machinery—for example, of the punched-card type—so that consideration should be given to the use of such equipment where it is available.

It may also be mentioned that two contour charts of the integrands in (6a), (6b), and (8), with the factor c_l or dc_l/dy omitted, have been prepared on film and may be obtained on request from the National Advisory Committee for Aeronautics. Their form is such that, if the transparency is superimposed on a correctly scaled drawing of the wing plan form, with a boundary point (x',y') at the origin of the chart, the contour value read at point (x,y) is the desired value of the integrand. The charts are satisfactorily accurate except in the neighborhood of the singularities.

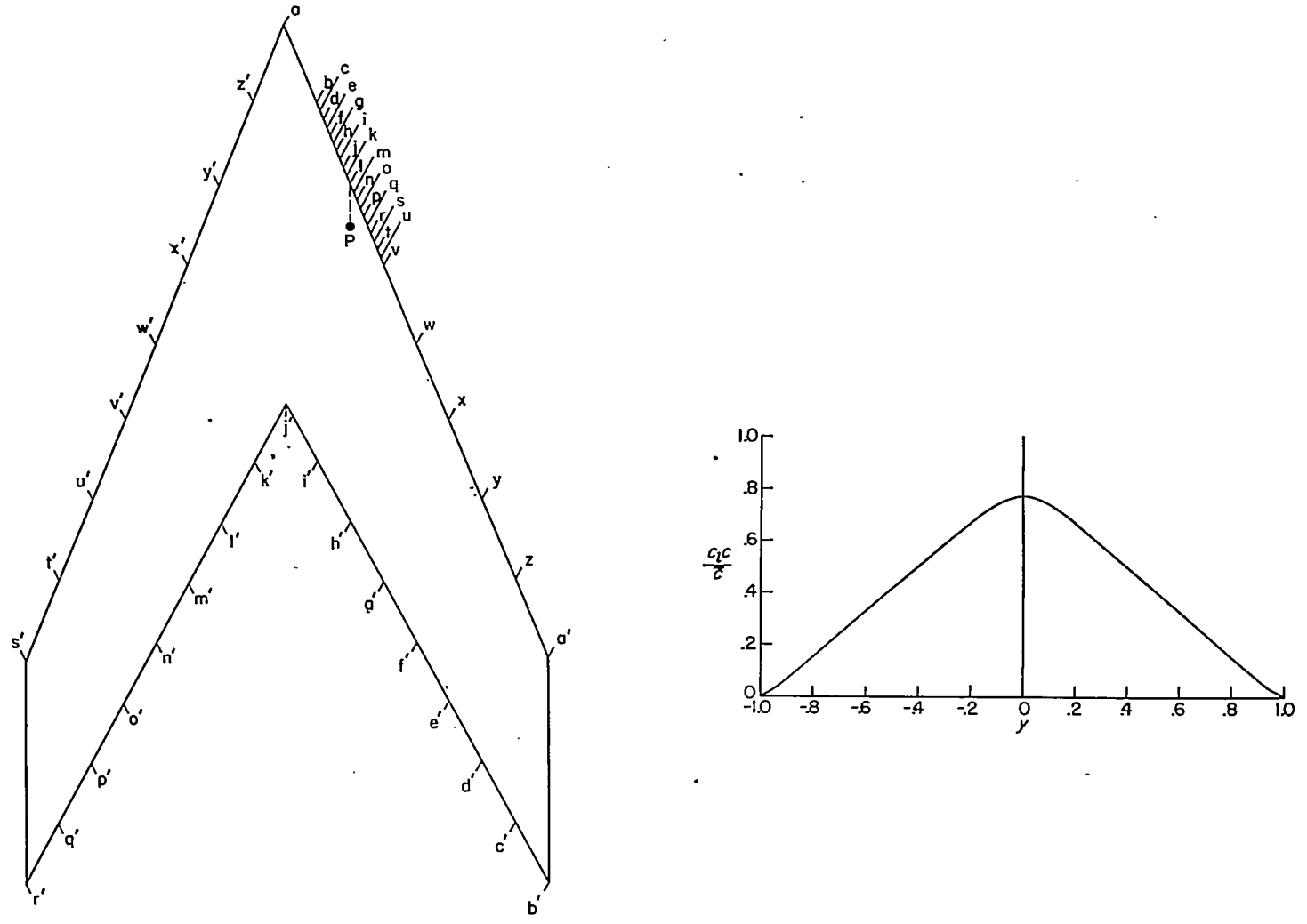

FIGURE 4.—Plan form and spanwise lift distribution of the wing for which example calculations are shown in table I and in figures 5 and 6.

TABLE I

COMPUTATION OF INTEGRANDS FOR INTEGRALS (7a), (7b), AND (8)
FOR POINT P (x=0.7707, y=0.2500) OF FIGURE 4

Boundary point, (x',y')	① $x-x'$	② $y-y'$	③ $\sqrt{①^2+②^2}$	④ cl	⑤ dc_l/dy'	⑥* $\frac{④}{③}\left[\frac{①}{③}+1\right]$	⑦** ④/③	⑧*** $\frac{⑤}{③}[⑥+①]$
a	0.7707	0.2500	0.8102	0.5880	0	4.5900	0.7259	0
b	.4660	.1250	.4825	.5725	−.214	9.0097	1.1874	−1.6238
c	.4355	.1125	.4498	.5700	−.228	9.9722	1.2672	−1.7942
d	.4051	.1000	.4173	.5669	−.244	11.1725	1.3585	−2.0067
e	.3746	.0875	.3847	.5637	−.259	12.7151	1.4653	−2.2475
f	.3441	.0750	.3522	.5604	−.273	14.7721	1.5911	−2.5345
g	.3137	.0625	.3199	.5569	−.289	17.6479	1.7409	−2.9298
h	.2832	.0500	.2876	.5536	−.300	21.9746	1.9249	−3.4248
i	.2527	.0375	.2555	.5501	−.316	29.1773	2.1530	−4.2824
j	.2223	.0250	.2237	.5459	−.331	43.5344	2.4403	−5.9050
k	.1918	.0125	.1922	.5419	−.344	86.6130	2.8195	−10.5677
l	.1613	0	.1613	.5373	−.360	----------	3.3329	----------
m	.1309	−.0125	.1315	.5329	−.373	−85.0679	4.0525	7.8300
n	.1004	−.0250	.1035	.5279	−.387	−41.5985	5.1005	3.1564
o	.0699	−.0375	.0793	.5225	−.401	−26.2156	6.5889	1.5954
p	.0394	−.0500	.0637	.5168	−.415	−16.7288	8.1130	.8557
q	.0090	−.0625	.0631	.5115	−.429	−9.3510	8.1062	.4949
r	−.0215	−.0750	.0780	.5059	−.444	−4.8863	6.4859	.3345
s	−.0520	−.0875	.1018	.5009	−.458	−2.8005	4.9204	.2607
t	−.0824	−.1000	.1296	.4947	−.470	−1.8017	3.8171	.2218
u	−.1129	−.1125	.1594	.4885	−.484	−1.2666	3.0646	.2001
v	−.1434	−.1250	.1902	.4831	−.498	−.9497	2.5363	.1865
w	−.4481	−.2500	.5131	.4123	−.634	−.2091	.8039	.1648
x	−.7527	−.3750	.8409	.3261	−.770	−.0912	.3879	.1811
y	−1.0574	−.5000	1.1697	.2206	−.902	−.0425	.1890	.2026
z	−1.3621	−.6250	1.4986	.1006	−1.005	−.0146	.0668	.2195
a′	−1.6668	−.7500	1.8278	0	−.380	0	0	.0816
b′	−2.5271	−.7500	2.6360	0	−.380	0	0	.0552
c′	−2.2941	−.6250	2.3777	.1006	−1.005	−.0056	.0421	.1344
d′	−2.0611	−.5000	2.1209	.2206	−.902	−.0125	.1042	.1079
e′	−1.8281	−.3750	1.8662	.3261	−.770	−.0177	.1748	.0782
f′	−1.5951	−.2500	1.6146	.4123	−.634	−.0200	.2555	.0495
g′	−1.3621	−.1250	1.3678	.4831	−.498	−.0162	.3527	.0227
h′	−1.1291	0	1.1291	.5373	−.360	0	.4761	0
i′	−.8961	.1250	.9048	.5725	−.214	.0439	.6322	−.0149
j′	−.6631	.2500	.7078	.5880	0	.1512	.8297	0
k′	−.8961	.3750	.9714	.5725	.214	.1182	.5888	.0432
l′	−1.1291	.5000	1.2349	.5373	.360	.0920	.4348	.0760
m′	−1.3621	.6250	1.4986	.4831	.498	.0705	.3228	.1088
n′	−1.5951	.7500	1.7626	.4123	.634	.0522	.2337	.1414
o′	−1.8281	.8750	2.0267	.3261	.770	.0365	.1608	.1748
p′	−2.0611	1.0000	2.2909	.2206	.902	.0221	.0960	.2070
q′	−2.2941	1.1250	2.5551	.1006	1.005	.0092	.0395	.2329
r′	−2.5271	1.2500	2.8193	0	.380	0	0	.0888
s′	−1.6668	1.2500	2.0834	0	.380	0	0	.1266
t′	−1.3621	1.1250	1.7666	.1006	1.005	.0206	.0572	.3610
u′	−1.0574	1.0000	1.4554	.2206	.902	.0602	.1512	.3586
v′	−.7527	.8750	1.1542	.3261	.770	.1296	.2824	.3533
w′	−.4481	.7500	.8737	.4123	.634	.2676	.4716	.3600
x′	−.1434	.6250	.6412	.4831	.498	.6010	.7545	.3966
y′	.1613	.5000	.5254	.5373	.360	1.4035	1.0219	.4931
z′	.4660	.3750	.5981	.5725	.214	2.7137	.9564	.6101

*Integrand for (7a)
**Integrand for (7b)
***Integrand for (8)

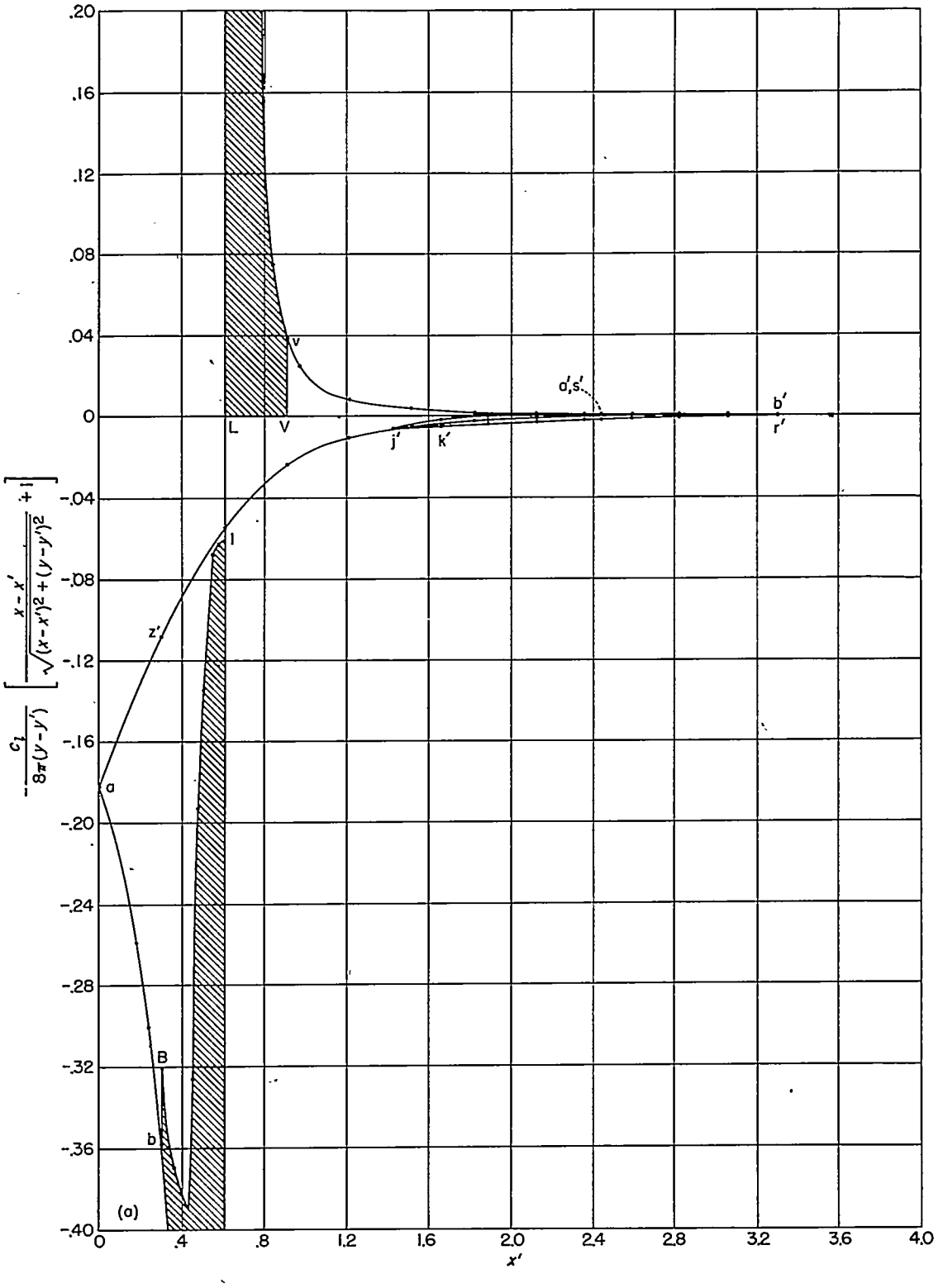

(a) Determination of integral (7a).

FIGURE 5.—Determination of the mean surface slope dz/dx at point P of the example wing of figure 4.

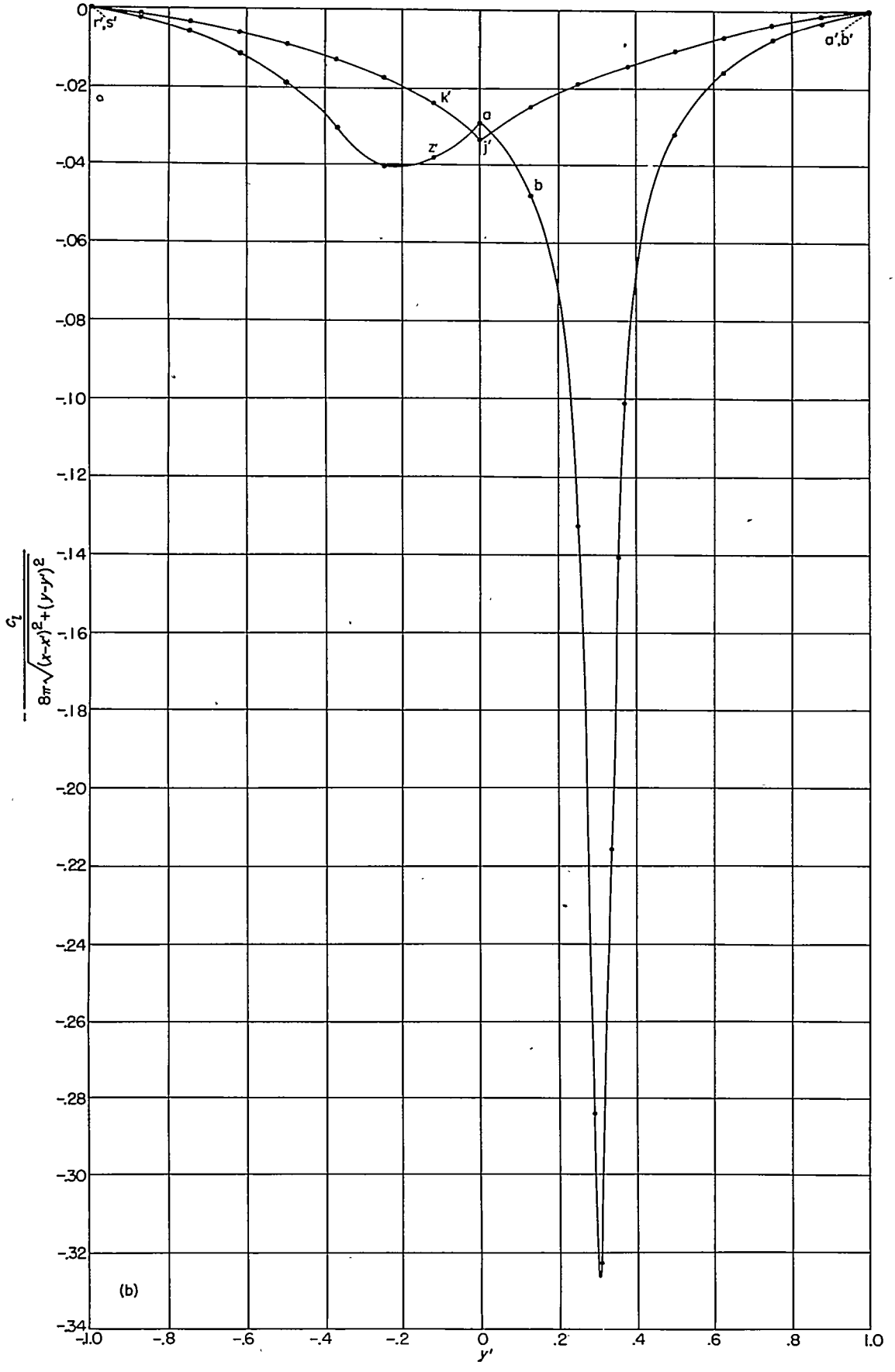

(b) Determination of integral (7b).

FIGURE 5.—Continued.

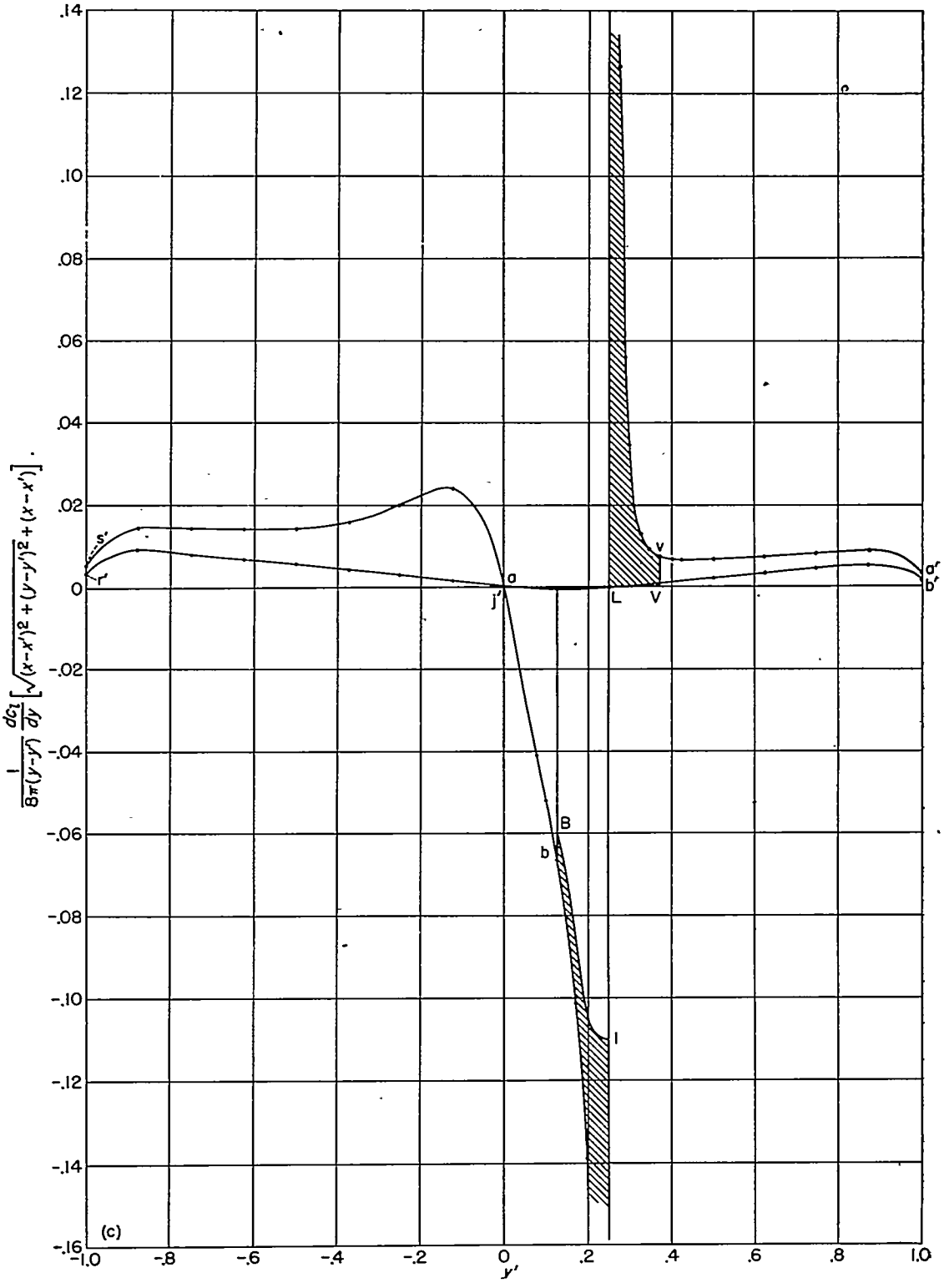

(c) Determination of integral (8).

FIGURE 5.—Concluded.

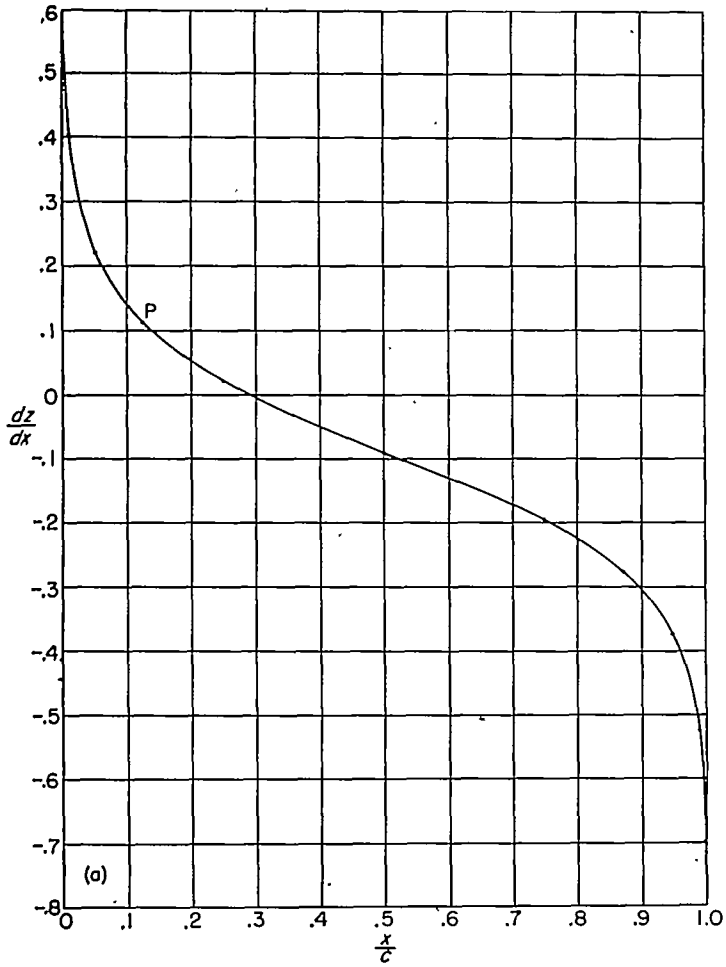

(a) Calculated slopes, example wing.

FIGURE 6.—Calculated slopes along streamwise mean camber line through point P (see fig. 4) and slopes along NACA $a=1.0$ mean line at $c_l=1.0$.

POLYGONAL WINGS WITH UNIFORM AREA LOADING

For a uniformly loaded wing (uniform chordwise loading and uniform c_l across the span) the boundary of which consists of a number of straight-line segments, the integrations to determine the local slope of the surface and the local height of the surface may both be done analytically. The previously derived equations can be integrated with respect to x' and y', where the point (x',y') moves from one end of the straight-line segment to the other. In the present development, however, the straight-line segment will be treated as a whole. The vertical induced velocity w due to the unit bounding vortex is expressed as the sum of w_A, w_B, . . ., the velocities due to the separate straight segments A, B, . . . (see fig. 7) which are given by the Biot-Savart law (eq. (4)). The contribution of segment A to the slope of the surface at point (x,y) is, therefore, $-\frac{C_L}{2}\int_{-\infty}^{x} w_A dx$ and the contribution to the height of the surface at the point (x,y) is

$$-\frac{C_L}{2}\int_{x_{LE}}^{x} dx \int_{-\infty}^{x} w_A dx$$

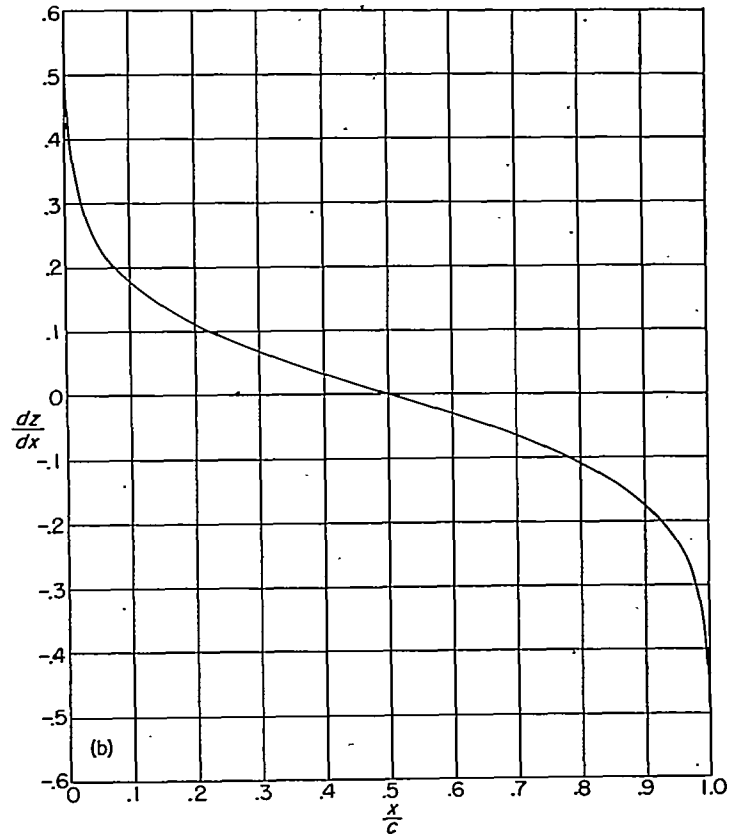

(b) Slopes along NACA $a=1.0$ mean line, for $c_l=1.0$, from reference 3.

FIGURE 6.—Concluded.

Summing these expressions for all the segments A, B, . . . gives the total slope or height of the mean camber surface at the desired point.

As already noted, these integrals for the separate straight segments can be evaluated analytically. Because the mathematical manipulation and the resulting formulas are somewhat lengthy, they are given in the appendix. Three different cases, distinguished by the relative geometry of the vortex segment (that is, the segment of the wing boundary) and the point (x,y) where the slope or height of the surface is to be found, are discussed in the appendix. In case I (fig. 8), the path of integration from $-\infty$ to x crosses the segment; in case II (fig. 9), the path of integration does not cross the segment; and in case III (fig. 10), which is a special case of II, the path of integration is parallel to the segment.

It should be noted that this same problem has been treated from a somewhat different viewpoint in reference 4.

COMPRESSIBILITY CORRECTION

If the mean camber surface is desired for a compressible subsonic flow at Mach number M, the Prandtl-Glauert method, as described in reference 5, may be used. That is, all the longitudinal (streamwise) dimensions of the wing are stretched by the factor $1/\sqrt{1-M^2}$, so that the aspect ratio is reduced by the factor $\sqrt{1-M^2}$ and the tangent of the sweep angle is increased by the factor $1/\sqrt{1-M^2}$, and the mean

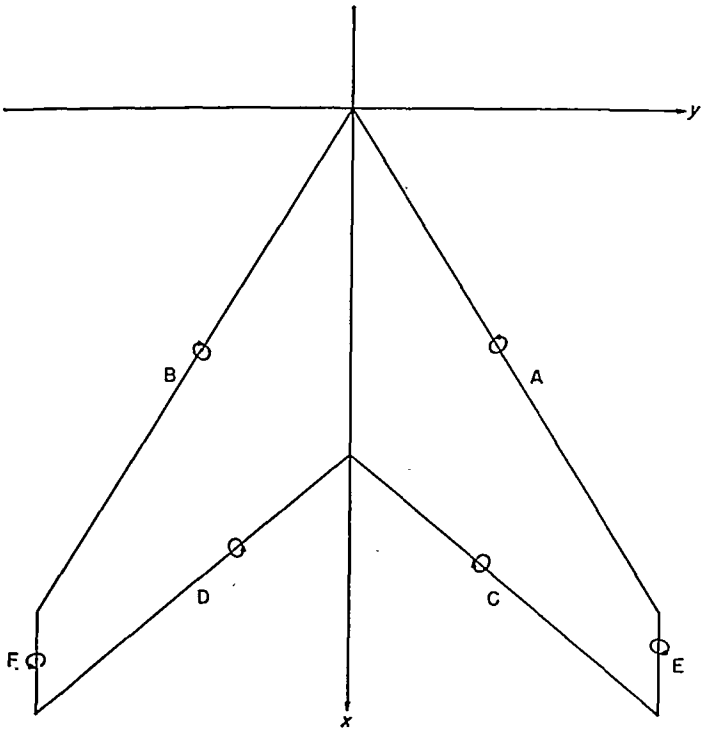

FIGURE 7.—Unit bounding vortex composed of separate straight segments A, B, C, D, E, and F superimposed on wing plan form boundary.

camber surface is calculated for this fictitious wing in incompressible flow at a lift coefficient equal to the desired lift coefficient multiplied by $1-M^2$. The ordinates (values of z) so obtained will be precisely the ordinates of the mean camber surface for the desired wing at the desired lift coefficient in the compressible flow at Mach number M.

EXAMPLES OF CALCULATED MEAN CAMBER SURFACES

Sweptback wing, $A=1.74$.—Figure 11 shows (by the curved lines) mean camber lines calculated for the wing already described in the example and in figure 4. The points where the slopes were computed are indicated by small circles. It should be noted that figure 11 and subsequent similar figures do not represent oblique projections of the wings. Rather, they show the true plan forms of the wings (in the xy-plane) and the true mean camber lines (parallel to the xz-plane); accordingly, the y- and z-axes coincide on the figures.

In figure 11 and the subsequent similar figures, all the leading-edge points have been assumed to lie along a horizontal line. This choice is, of course, arbitrary; that is, the extent to which the present linear theory is applicable would be essentially unaltered if, for example, the wing had a reasonable amount of dihedral.

Uniformly loaded triangular wing.—The formulas derived in the appendix for cases I and II were used to calculate the mean camber surface of a triangular wing having an angle of sweep of 68.4° of the leading edge (aspect ratio, 1.57) such that the wing should be uniformly loaded at unit lift coefficient in incompressible flow. Figure 12 shows the plan form and the chordwise camber lines for several spanwise stations. The dimensions shown correspond to a root chord of unity; however, the z-scale is shown somewhat exaggerated.

Uniformly loaded swept wing.—The formulas derived for cases I, II, and III were used to calculate the mean camber surface of a swept wing of aspect ratio 8, taper ratio 0.45 and 45° sweepback of the quarter-chord line such that the wing should be uniformly loaded at unit lift coefficient at a Mach number of 0.9. In accordance with the proposed method of taking into account compressibility, the calculations were made for the stretched wing in incompressible flow. The stretching factor is $\frac{1}{\sqrt{1-(0.9)^2}}=2.29$, so that the aspect ratio of the stretched wing is 3.5 and the sweep of the quarter-chord line is 66.46°. Figure 13 (a) shows this stretched wing and the mean camber lines calculated for this stretched wing in incompressible flow at unit lift coefficient. The dimensions shown correspond to a semispan of unity; however, the z-scale is shown somewhat reduced. The corresponding mean camber lines for the physical wing ($A=8$; design $C_L=1.0$ at $M=0.9$) should have 44 percent as much camber as the mean camber lines for this stretched wing in the incompressible flow.

Swept wing with elliptical span load distribution.—For the wing plan form of the preceding example another mean camber surface was calculated that, at unit lift coefficient and a Mach number of 0.9, would give uniform chordwise loading but an elliptical span load distribution for the wing as a whole. Mean camber lines for this case are presented in figure 13 (b).

This example was also calculated, under the direction of Mr. Robert R. Graham of the Langley Laboratory, by the method of reference 1. The two results were in very good agreement. No definite information was obtained, however, with regard to the relative expediency of the two methods (that of ref. 1 and that of the present report). One might suppose that the present method would be preferable for wings with uniform chordwise loading, since it is designed to take advantage of this particular characteristic. The work represented by table I and figure 5 (outlining the computations for the slope at one point), however, is by no means small, so that such a presumption is not definitely substantiated by present experience. Perhaps the fact that the computations and integrations are of such form that they can be readily performed by modern high-speed computing machinery constitutes the most significant characteristic of the present method.

LANGLEY AERONAUTICAL LABORATORY,
NATIONAL ADVISORY COMMITTEE FOR AERONAUTICS,
LANGLEY FIELD, VA., *January 13, 1953.*

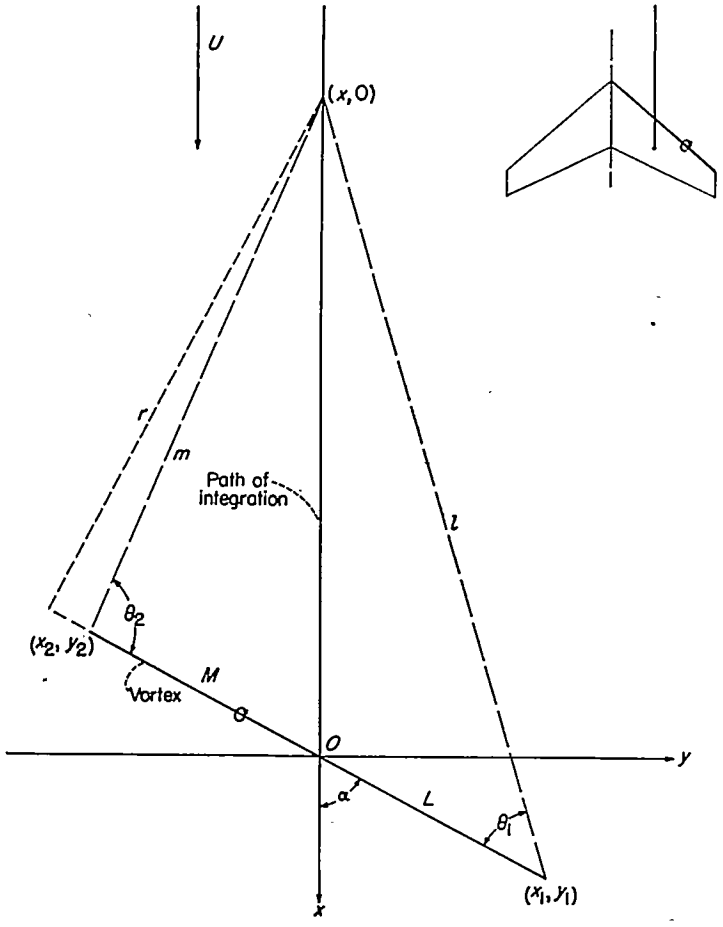

FIGURE 8.—Geometrical relationships for case I. Heavy lines in small sketch show relative positions of vortex segment and path of integration for this case.

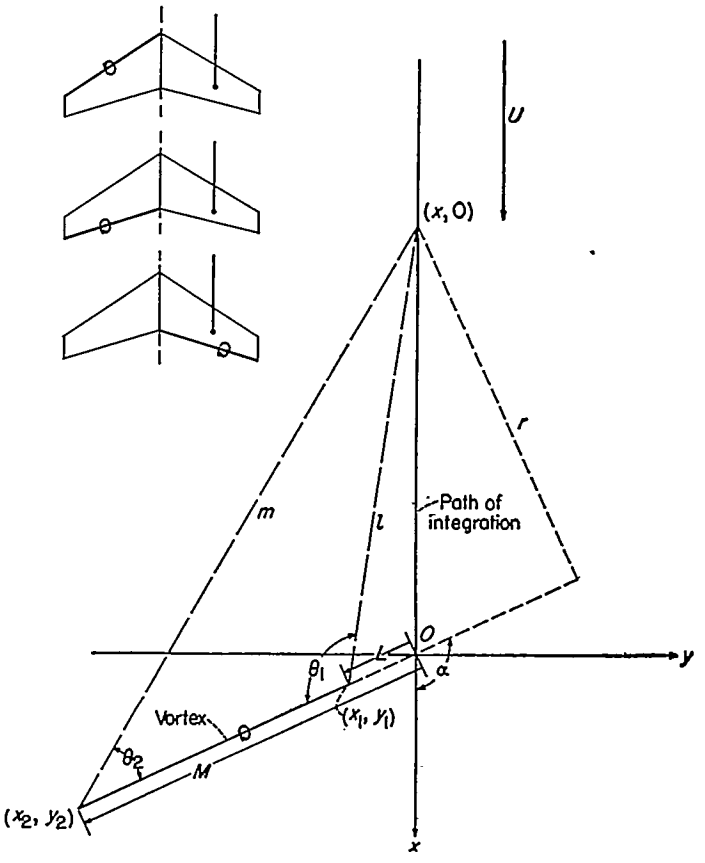

FIGURE 9.—Geometrical relationships for case II. Heavy lines in small sketches show relative positions of vortex and path of integration for three different conditions for which this case applies.

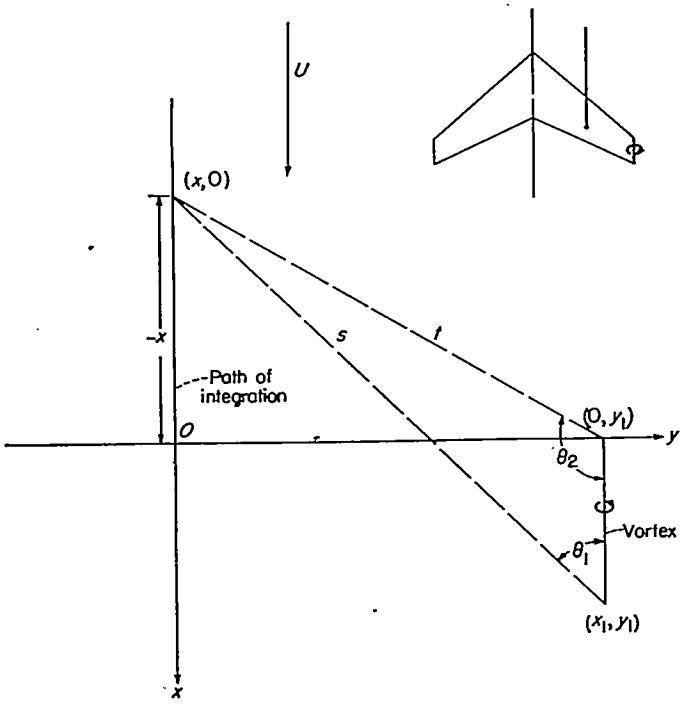

FIGURE 10.—Geometrical relationships for case III. Heavy lines in small sketch show relative positions of vortex segment and path of integration for this case.

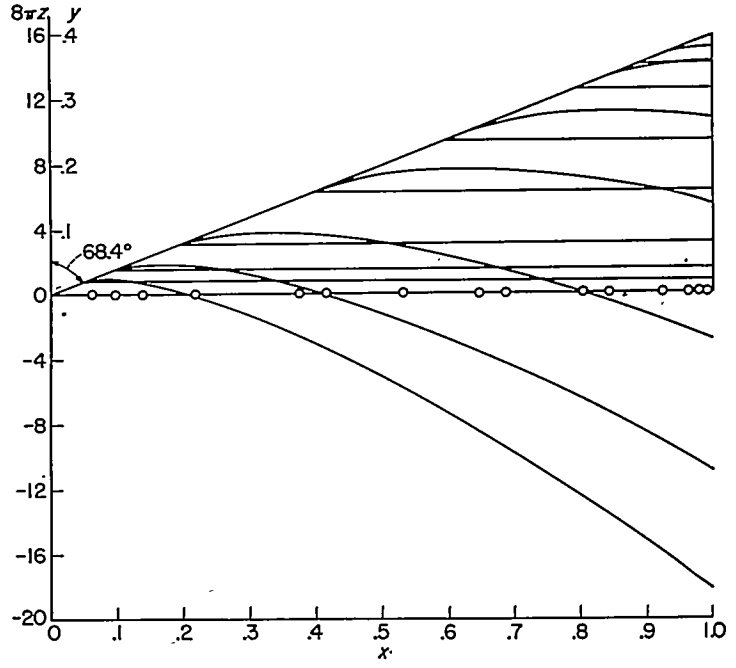

FIGURE 12.—Chordwise mean camber lines at several spanwise stations for a triangular wing with uniform area loading. Leading-edge sweep angle, 68.4°; C_L=1.0; aspect ratio, 1.57.

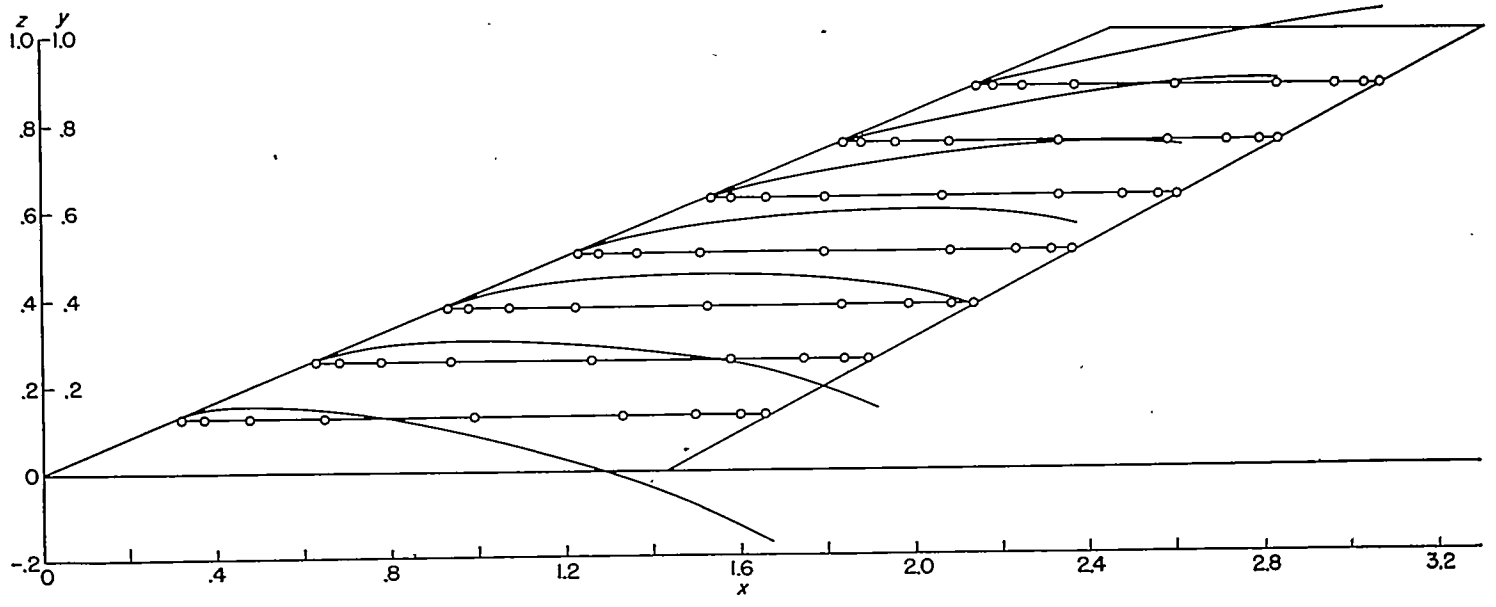

FIGURE 11.—Mean camber lines for the wing of figure 4 in incompressible flow. Aspect ratio, 1.74; taper ratio, 0.6; quarter-chord sweep angle, 66.46°.

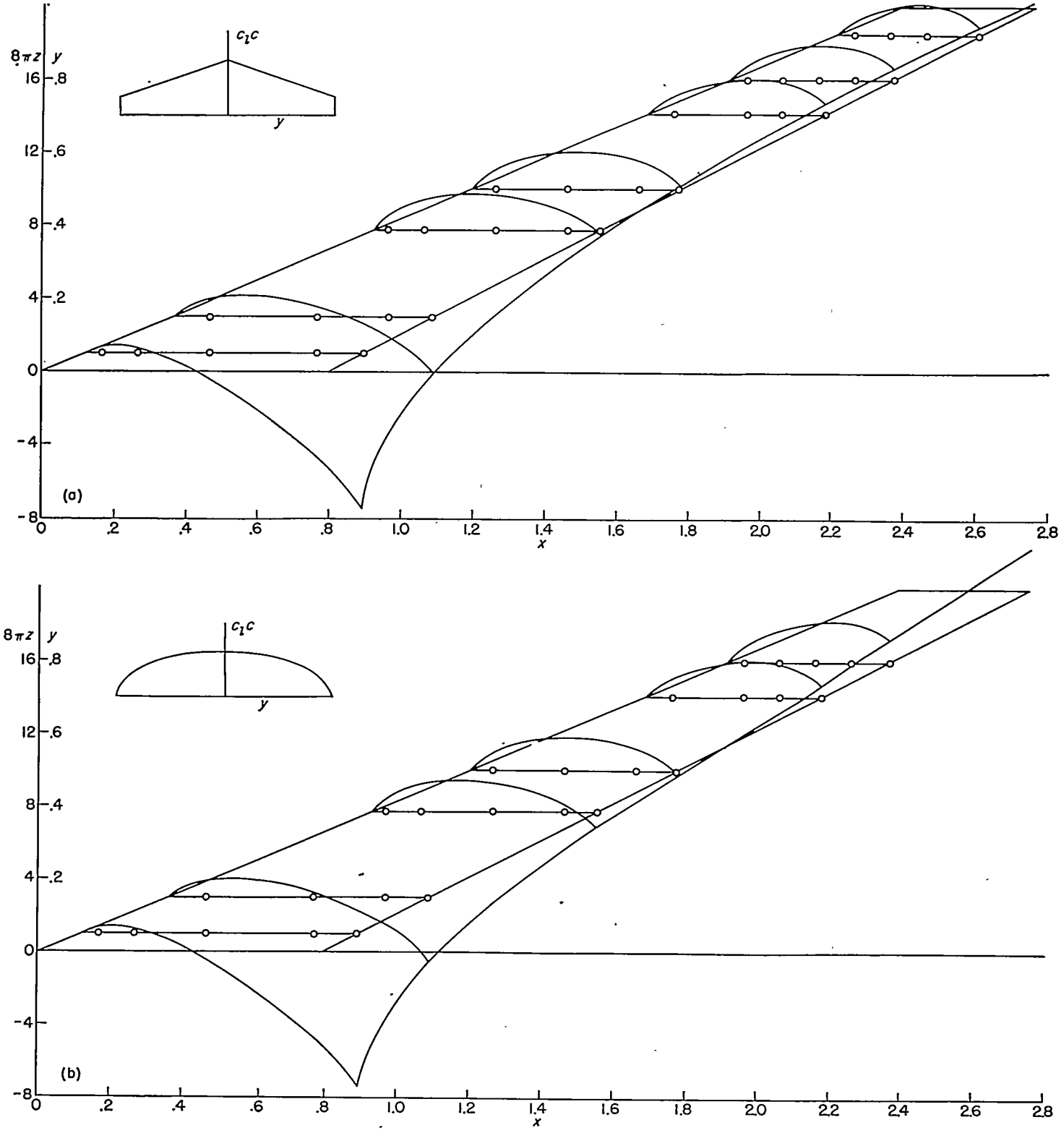

(a) Uniform area loading.

(b) Uniform chordwise loading; elliptical span load distribution.

FIGURE 13.—Mean camber lines for the stretched wing at unit lift coefficient in incompressible flow. Aspect ratio, 3.5; taper ratio, 0.45; quarter-chord sweep angle, 66.46°; $C_L=1.0$. For the physical wing (aspect ratio, 8; taper ratio, 0.45; quarter-chord sweep angle, 45°) with unit lift coefficient at $M=0.9$, the mean camber lines should have 44 percent as much camber as the lines shown here. Small figures show span load distributions. Circles indicate points for which z was computed.

APPENDIX

DEVELOPMENT OF FORMULAS FOR UNIFORMLY LOADED POLYGONAL WINGS

Case I—Path of integration crosses vortex segment.—If the vortex segment is the leading edge of the wing, the path of integration may cross it. The vortex segment and the path of integration for this case are shown by the heavy lines in the small sketch in figure 8. The integral $\int_{-\infty}^{x} w_I dx$ is improper because the integrand becomes infinite where the path of integration crosses the vortex. The Cauchy principal value, however, can be determined. Before the integration is performed, the Biot-Savart formula (eq. (4)) is expressed in terms of the variable x and the fixed dimensions of the vortex segment, where the origin is defined as the point of intersection of the path of integration and the vortex segment. Accordingly, the end points of the vortex segment are (x_1,y_1) and (x_2,y_2), where $y_1>y_2$ (see fig. 8). Let

$$L=y_1 \csc \alpha$$

$$M=-y_2 \csc \alpha$$

$$\alpha=\tan^{-1}\left(\frac{y_1-y_2}{x_1-x_2}\right)$$

Then it can be seen that

$$r=x \sin \alpha$$

$$\cos \theta_1=\frac{L-x \cos \alpha}{l}=\frac{L-x \cos \alpha}{\sqrt{x^2-2xL \cos \alpha+L^2}}$$

$$\cos \theta_2=\frac{M+x \cos \alpha}{m}=\frac{M+x \cos \alpha}{\sqrt{x^2+2xM \cos \alpha+M^2}}$$

The contribution of w_I to the slope of the mean camber surface will be

$$\left(\frac{dz}{dx}\right)_I=-\frac{1}{2} C_L \int_{-\infty}^{x} w_I dx$$

$$=-\frac{1}{2} C_L \int_{-\infty}^{x} \frac{1}{4\pi x \sin \alpha}\left(\frac{L-x \cos \alpha}{\sqrt{x^2-2xL \cos \alpha+L^2}}+\right.$$

$$\left.\frac{M+x \cos \alpha}{\sqrt{x^2+2xM \cos \alpha+M^2}}\right) dx$$

$$=\frac{-C_L}{8\pi \sin \alpha}\left\{\cos \alpha \log_e\left[\left(\frac{L^2}{M^2}\right)\left(\frac{x+M \cos \alpha+m}{x-L \cos \alpha+l}\right)\right]+\right.$$

$$\left.\log_e\left[\frac{x^2 \sin^2 \alpha}{(l+L-x \cos \alpha)(m+M+x \cos \alpha)}\right]\right\} \qquad \text{(A1)}$$

It is of interest to note that, along the wing tip or the wing root, where L or M goes to zero while x is positive, this slope becomes infinite.

The contribution to the height of the mean camber surface will be the integral of this last expression; that is,

$$z_I=\int_0^x \left(\frac{dz}{dx}\right)_I dx$$

$$=\frac{-C_L}{8\pi \sin \alpha}\left\{x \cos \alpha \log_e \frac{L^2}{M^2}+2x \log_e \sin \alpha+x \log_e x^2+\right.$$

$$(x \cos \alpha-M \sin^2 \alpha) \log_e (x+M \cos \alpha+m)-$$

$$(x \cos \alpha+L \sin^2 \alpha) \log_e (x-L \cos \alpha+l)-$$

$$\left.x \log_e (m+M+x \cos \alpha)(l+L-x \cos \alpha)+\cos \alpha(l-m)\right\}\Bigg|_0^x \qquad \text{(A2)}$$

or, after substituting the indicated limits,

$$z_I=\frac{-C_L}{8\pi \sin \alpha}\left\{x \cos \alpha \log_e \frac{L^2}{M^2}+2x \log_e \sin \alpha+x \log_e x^2+\right.$$

$$(x \cos \alpha-M \sin^2 \alpha) \log_e (x+M \cos \alpha+m)-$$

$$(x \cos \alpha+L \sin^2 \alpha) \log_e (x-L \cos \alpha+l)-$$

$$x \log_e (m+M+x \cos \alpha)(l+L-x \cos \alpha)+$$

$$M \sin^2 \alpha \log_e M(1+\cos \alpha)+$$

$$\left.L \sin^2 \alpha \log_e L(1-\cos \alpha)+[(l-m)-(L-M)] \cos \alpha\right\} \qquad \text{(A3)}$$

Case II—Path of integration does not cross vortex segment.—The three small sketches in figure 9 show three cases in which the path of integration does not cross the vortex segment. In two of these cases, the segment lies along the trailing edge; in the third case, the segment lies along the leading edge but lies wholly to one side of the path of integration.

For the derivation of the formulas for case II, the origin of coordinates is specified as the intersection of the path of integration with the vortex or with the line of the vortex extended. The end points of the vortex segment are again designated (x_1,y_1) and (x_2,y_2), where $y_1>y_2$. The angle α is defined as before. Following the sign convention indicated in figure 8, M will be considered positive if (x_2,y_2) lies to the left of the origin, and L will be considered positive if (x_1,y_1) lies to the right of the origin. For example, in figure 9, L is a negative quantity, whereas M is a positive quantity.

For any of the three cases shown in figure 9, the expression for w_{II} is identical with that for w_I. Furthermore, the expression for

$$\left(\frac{dz}{dx}\right)_{II}=-\frac{C_L}{2}\int_{-\infty}^{x} w_{II} dx$$

is identical in form with the expression (A1) derived for $\left(\frac{dz}{dx}\right)_I$; that is, neither singular points in the integration nor negative values of x, L, or M affect the expression for the integral.

Integrating $\left(\frac{dz}{dx}\right)_{II}$ in order to obtain z_{II} yields the same expression for the indefinite integral as was found in integrating $\left(\frac{dz}{dx}\right)_{I}$, so that the only differences between the expressions for z_{II} and z_{I} arise from the different limits of integration—for z_{I}, the limits were 0 and x, whereas for z_{II}, the limits are x_{LE} and x; that is,

$$z_{II}=\int_{x_{LE}}^{x}\left(\frac{dz}{dx}\right)_{II}dx$$

$$=\frac{-C_L}{8\pi\sin\alpha}\Big\{x\cos\alpha\log_e\frac{L^2}{M^2}+2x\log_e\sin\alpha+x\log_e x^2+$$

$$(x\cos\alpha-M\sin^2\alpha)\log_e(x+M\cos\alpha+m)-$$

$$(x\cos\alpha+L\sin^2\alpha)\log_e(x-L\cos\alpha+l)-$$

$$x\log_e(m+M+x\cos\alpha)(l+L-x\cos\alpha)+\cos\alpha(l-m)\Big\}\Big|_{x_{LE}}^{x} \tag{A4}$$

Case III—Vortex segment parallel to free stream and hence to path of integration (fig. 10).—Coordinates are chosen so that the path of integration lies along $y=0$. The end points of the vortex segment are $(0, y_1)$ and (x_1, y_1) where $x_1>0$.

Then, from figure 10,

$$s=\sqrt{(x_1-x)^2+y_1^2}$$

$$t=\sqrt{x^2+y_1^2}$$

$$\cos\theta_1=\frac{x_1-x}{s}=\frac{x_1-x}{\sqrt{(x_1-x)^2+y_1^2}}$$

$$\cos\theta_2=\frac{x}{t}=\frac{x}{\sqrt{x^2+y_1^2}}$$

Then

$$\left(\frac{dz}{dx}\right)_{III}=-\frac{C_L}{2}\int_{-\infty}^{x}w_{III}\,dx$$

$$=-\frac{C_L}{8\pi y_1}\int_{-\infty}^{x}\left[\frac{x_1-x}{\sqrt{(x_1-x)^2+y_1^2}}+\frac{x}{\sqrt{x^2+y_1^2}}\right]dx$$

$$=-\frac{C_L}{8\pi y_1}\left[\sqrt{x^2+y_1^2}-\sqrt{(x_1-x)^2+y_1^2}+x_1\right] \tag{A5}$$

and

$$z_{III}=-\frac{C_L}{16\pi y_1}\Big(\{(x_1-x)\sqrt{(x_1-x)^2+y_1^2}+x\sqrt{x^2+y_1^2}+$$

$$y_1^2\log_e[x_1-x+\sqrt{(x_1-x)^2+y_1^2}]+$$

$$y_1^2\log_e(x+\sqrt{x^2+y_1^2})\}-\{(x_1-x_{LE})\sqrt{(x_1-x_{LE})^2+y_1^2}+$$

$$x_{LE}\sqrt{x_{LE}^2+y_1^2}+y_1^2\log_e[x_1-x_{LE}+\sqrt{(x_1-x_{LE})^2+y_1^2}]+$$

$$y_1^2\log_e[x_{LE}+\sqrt{x_{LE}^2+y_1^2}+2x_1(x-x_{LE})]\}\Big) \tag{A6}$$

For equations (A5) and (A6), the direction of rotation of the vortex segment was assumed to be that corresponding to the right wing tip. For the left wing tip, the signs should be reversed. Stated differently, the equations will be correct in either case if y_1 in the first factor on the right-hand side is replace by $|y_1|$.

REFERENCES

1. Cohen, Doris: A Method for Determining the Camber and Twist of a Surface To Support a Given Distribution of Lift, With Applications to the Load Over a Sweptback Wing. NACA Rep. 826, 1945. (Supersedes NACA TN 855.)
2. Milne-Thomson, L. M.: Theoretical Aerodynamics. D. Van Nostrand Co., Inc., or Macmillan and Co., Ltd., 1948.
3. Abbott, Ira H., Von Doenhoff, Albert E., and Stivers, Louis S., Jr.: Summary of Airfoil Data. NACA Rep. 824, 1945. (Supersedes NACA WR L-560.)
4. Lampert, Seymour: Conical Flow Methods Applied to Uniformly Loaded Wings in Subsonic Flow. Jour. Aero. Sci., vol. 18, no. 2, Feb. 1951, pp. 107–114.
5. Hess, Robert V., and Gardner, Clifford S.: Study by the Prandtl-Glauert Method of Compressibility Effects and Critical Mach Number for Ellipsoids of Various Aspect Ratios and Thickness Ratios. NACA TN 1792, 1949.